nature COMMUNICATIONS

ARTICLE

Received 15 Jul 2010 | Accepted 5 Oct 2010 | Published 16 Nov 2010

DOI: 10.1038/ncomms1106

Overlap between folding and functional energy landscapes for adenylate kinase conformational change

Ulrika Olsson[1] & Magnus Wolf-Watz[1]

Enzyme function is often dependent on fluctuations between inactive and active structural ensembles. Adenylate kinase isolated from *Escherichia coli* (AK_e) is a small phosphotransfer enzyme in which interconversion between inactive (open) and active (closed) conformations is rate limiting for catalysis. AK_e has a modular three-dimensional architecture with two flexible substrate-binding domains that interact with the substrates AMP, ADP and ATP. Here, we show by using a combination of biophysical and mutagenic approaches that the interconversion between open and closed states of the ATP-binding subdomain involves partial subdomain unfolding/refolding in an otherwise folded enzyme. These results provide a novel and, possibly general, molecular mechanism for the switch between open and closed conformations in AK_e.

[1] Department of Chemistry, Chemical Biological Centre, Umeå University, Umeå 90187, Sweden. Correspondence and requests for materials should be addressed to M.W.-W. (email: magnus.wolf-watz@chem.umu.se).

Structural plasticity in proteins is intimately linked to their function. For example, the activity of many signal transducing enzymes is associated with large conformational changes between active and inactive states[1,2]. Moreover, many proteins undergo significant conformational changes on interaction with target proteins or small ligands[3,4]. In analogy to the energy landscape model of protein folding[5], transitions between native conformational states in folded proteins are thought to be achieved through multiple pathways[6,7]. Qualitative descriptions of conformational changes can be inferred from analysis of the stable ground states. Hinge and shear motions, and combinations thereof, have been proposed to facilitate conformational changes[8]. What is not yet clear is the molecular mechanism, including information on transition states and other transient intermediates, of conformational change in the native states of proteins. It is difficult to probe intermediates and transition states involved in conformational changes, as these states are short lived and not directly accessible by spectroscopy. Here, we describe experiments that allow us to decipher the molecular mechanism of a large-scale conformational change in adenylate kinase (AK).

AK catalyses the reversible phosphoryl transfer reaction $Mg^{2+}ATP + AMP \leftrightarrow Mg^{2+}ADP + ADP$ and has the primary role of maintaining the energy balance in cells. The importance of AK is reflected in its ubiquitous presence in many different organisms and tissues[9]. AK isolated from *E. coli* (AK_e) uses a random bi–bi mechanism during catalysis[10,11] and the phosphoryl transfer chemistry likely follows an associative mechanism[12]. A simplified nucleotide-binding mechanism for AK is shown in Figure 1.

The structure of AK_e has been solved in substrate-free (open)[13] and inhibitor P^1,P^5–Di(adenosine-5′)pentaphosphate (Ap5A[14])-bound (closed) conformations[15] (Fig. 1). NMR experiments conducted in our laboratory have shown that the closed conformation represents the catalytically active state in which phosphoryl transfer occurs[16]. AK_e is a modular enzyme and consists of a CORE subdomain and ATP- and AMP-binding subdomains (Fig. 1). Both ATP and AMP subdomains (ATP_{lid} and AMP_{lid}) undergo significant conformational changes in response to substrate binding. The large conformational change has at least two functional origins: first, the active site must be dehydrated to avoid non-productive hydrolysis of ATP and, second, the substrates are aligned optimally for the phosphoryl-transfer chemistry. The local thermodynamic stability of the nucleotide-binding subdomains is significantly lower compared with the CORE, and the subdomains fold and unfold in a non-cooperative manner[17]. From a functional perspective, this feature allows the rearrangement in backbone hydrogen bonding patterns (observed during the open-to-closed transition) without provoking global unfolding of the entire protein. It was recently reported that, at temperatures above 35 °C, the INSERT segment in ATP_{lid} (Fig. 1) selectively unfolded, resulting in reduced Ap5A-binding affinity[18]. The state with an unfolded INSERT segment was denoted as a 'binding incompetent state' and appears to be an intermediate on the global unfolding pathway. Selective unfolding of INSERT agrees with our previous observation that ATP_{lid} can be selectively unfolded without perturbing the structure of other parts of the enzyme[17].

The structural plasticity of AK_e is strongly coupled to its catalytic efficiency, as reopening of substrate binding domains with bound nucleotides is rate limiting for catalysis[19]. This observation is consistent with the finding that the rate-limiting step involves dissociation of bound nucleotides[10]. Notably, the conformational changes of ATP_{lid} and AMP_{lid} occur even in the absence of substrates[20]. Addition of ATP and AMP gradually shifts the conformational equilibrium towards the closed state[16]. Apparently, the conformational dynamics that is relevant for substrate binding is an intrinsic property of AK_e. This feature of enzyme function has also been observed for dihydrofolate reductase[21], cyclophilin A[22] and RNase A[23].

There exist two contradicting models for the open/closed conformational change of the nucleotide-binding subdomains in AK:

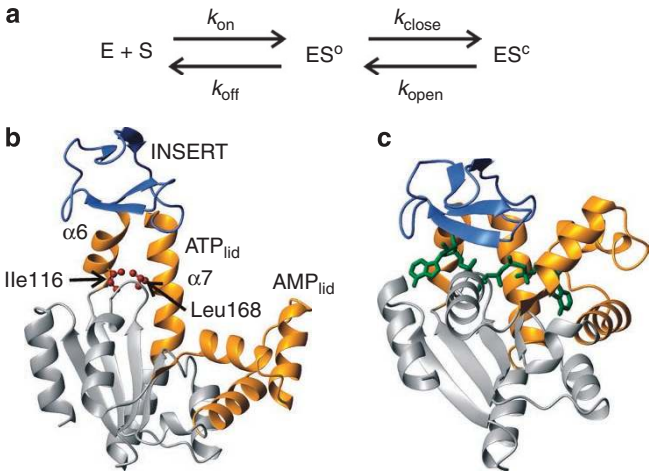

Figure 1 | Kinetic and structural models for substrate binding by AK. (**a**) Nucleotide binding mechanism for AK. E corresponds to enzyme, S to substrate, ES^O to a transient substrate-bound encounter complex, ES^C to the active conformation of AK. Superscripts 'O' and 'C' refer to AK in open (inactive) and closed (active) conformations. The rate constants for association and dissociation of ES^O are given by k_{on} and k_{off}, whereas the rate constants for conformational change are given by k_{close} and k_{open}. (**b**, **c**) Structures of AK_e during the extreme stages of catalysis. ATP_{lid} (residues 113–176) and AMP_{lid} (residues 28–72) are coloured gold and the INSERT segment of the ATP_{lid} (residues 122–159[43]) is coloured blue. (**b**) Substrate-free open AK_e (4AKE.pdb). Residues isoleucine 116 and leucine168, which are mutated into glycine in this study, are highlighted with ball and stick representations, and the location of alpha helices, α6 and α7, is indicated. (**c**) Closed AK_e with bound Ap5A (1AKE.pdb). All molecular graphic images in this report were prepared with MolMol[44].

(i) 'induced fit' and (ii) 'cracking' models. On the basis of an analysis of crystallographic structures, the induced fit model has been proposed for closure of both ATP_{lid} and AMP_{lid}. In this model, segments in between hinge regions are spatially translated as rigid bodies[24]. Closure of ATP_{lid} is accomplished by rotation of the INSERT segment around helices α6 and α7, which in turn rotate around the CORE (Fig. 1). In the 'cracking' model, significant strain energy is built up for residues in α6 and α7 during the reaction, and, at the transition state, this strain is released by a local unfolding event. At the downhill side of the activation energy barrier, the protein refolds and the thermodynamic minimum corresponding to the closed state is reached[25,26]. The cracking model was inferred from coarse-grained modelling and the principle of minimal frustration[26]. There are no experimental studies verifying which mechanism is used by AK. We previously identified a hydrophobic cluster in ATP_{lid} that consists of isoleucine (Ile) 116, valine (Val) 117, Val 164 and leucine (Leu) 168. Simultaneous mutation of these positions to glycine selectively unfolded the entire ATP_{lid} without perturbing the structures of the CORE and AMP_{lid} subdomains[17]. Surprisingly, this variant is capable of binding the inhibitor Ap5A (unpublished results). The hydrophobic cluster constituted of these four residues is conserved in the AK family, as evident from a published sequence alignment of 250 AK sequences[27].

On the basis of our observations on the quadruple mutant, we have, in this study, designed single (Ile116Gly, 'M1') and double (Ile116Gly and Leu168Gly, 'M2') mutated variants of AK_e in order to probe the reaction mechanism of ATP_{lid} closure. Our data show that segments in ATP_{lid} unfold and subsequently refold during the open-to-closed conformational transition, and show that folding and function are closely coupled events in AK_e.

Results

Structure of mutated AK_e in apo states. The structures of M1 and M2 AK_e variants were assessed with far-ultraviolet circular dichroism (CD) spectroscopy (Supplementary Fig. S1). Wild-type (WT) AK_e displays two distinct minima in the CD signal at 208 and 222 nm, in agreement with previous results[28]. Single and double mutations decrease the helical content of AK_e, as inferred from a reduction in the intensity of CD signals at 208 and 220 nm. As discussed below, this effect is dependent on selective destabilization/unfolding of α6 and α7. A qualitative analysis of the CD spectra using CDNN software (copyright Dr Gerald Böhm) provided deconvoluted helical contents of 64, 54 and 39 (±5) % for WT, M1 and M2, respectively. The reduction of helical content in M2 compared with WT AK_e is consistent with a complete loss of the helical structure of α6 and the section of α7 belonging to the ATP_{lid}. Taking the helical contents of WT AK_e and M2 as benchmarks for folded and unfolded α6 and α7, M1 is placed in between with a fraction of folded α6, α7 of ~60%.

^1H-^{15}N Heteronuclear Single-Quantum Coherence (HSQC) spectra of the two mutants superimposed on the WT are shown in Figure 2a,b. A visual inspection shows that M1 resembles the WT enzyme with many overlapping peaks distributed over the whole spectrum. In contrast, M2 shows marked spectral differences, compared with the WT enzyme.

Combined absolute differences in ^1H and ^{15}N chemical shifts between the M1 mutant and WT AK_e are shown in Figure 3a, and these results are plotted on the open AK_e structure in Figure 3b. Significant chemical shift differences are found in α6, α7, and these are propagated to a large part of the CORE. In light of the results from CD spectroscopy and from our previous analysis of a quadruple AK_e mutant[17], the chemical shift perturbations in α6 and α7 depend on a local unfolding event. The differences observed in the CORE are not dependent on unfolding, as we have shown that the quadruple mutant does not affect the topology of this domain[17]. The region of the CORE that shows shift changes (Fig. 3b,c) is part of a dense interaction network, and the observed changes may be reflecting minute changes in the packing of hydrophobic side chains. Interestingly, residues in the INSERT segment show no significant chemical shift perturbations in M1 (Fig. 3d), showing that this part of the molecule is structurally unaffected by the mutation. This result suggests that ATP_{lid} is composed of two cooperatively folding units: the INSERT and α6, α7 parts.

Partial assignments were obtained for the M2 mutant. The resonances corresponding to the ATP_{lid} could not be assigned because of unfolding of this subdomain. On the basis of spectral similarities with published NMR spectra of a quadruple mutant[17], we conclude that M2 has an unfolded ATP_{lid} subdomain (in agreement with the CD results). On the other hand, many residues in the CORE and AMP_{lid} could be assigned. In a spectrum recorded at 15 °C, resonances corresponding to the INSERT segment appeared at resonance frequencies very close to that of WT at the same temperature (Fig. 2c). This result implies that the INSERT retains the WT structure at 15 °C and that the absence of these resonances at 25 °C is due to conformational fluctuations on the μs–ms time scale. Notably, resonances corresponding to α6 and α7 could not be observed at 15 °C. The decoupling between folding of α6, α7 and the INSERT is thus a conserved feature of both M1 and M2 variants.

Protein stability was studied by measuring thermal stability, which provides melting points (T_m) and enthalpies of unfolding (ΔH_{vH}) at T_m. Unfolding curves for the three AK_e variants (Fig. 4) were fitted to a two-state unfolding transition according to Equation (3). Both mutated variants show a modest decrease in T_m compared with the WT (Supplementary Table S1); however, the ΔH_{vH} is significantly lower for both mutants. The large enthalpic difference is consistent with an unfolded ATP_{lid} for the mutants at T_m. The small effect on T_m in light of the large enthalpic differences between WT and mutants is explained with the thermal transition being dominated by the CORE subdomain.

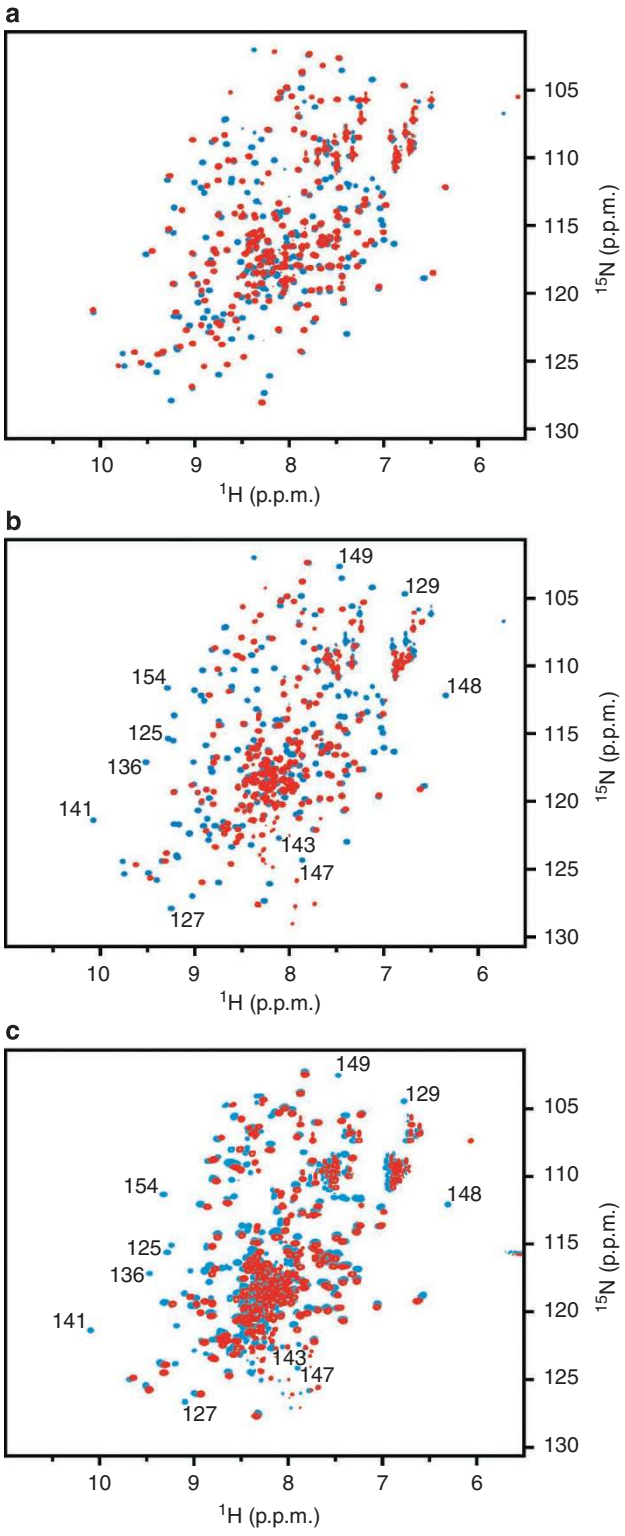

Figure 2 | NMR spectra of substrate-free WT AK_e, M1 and M2 mutants. In (**a**) and (**b**), WT AK_e is shown with blue contouring and the two mutants are contoured red. (**a**) Superimposition of ^1H-^{15}N HSQC spectra of WT AK_e and M1 acquired at 25 °C. (**b**) Superimposition of ^1H-^{15}N HSQC spectra of WT AK_e and M2 acquired at 25 °C. Selected resonances in the INSERT segment of the ATP_{lid} that are missing in the M2 mutant are indicated. (**c**) Superimposition of ^1H-^{15}N HSQC spectra of M2 acquired at 25 °C (red contours) and 15 °C (blue contours). Selected resonances (same set as in **b**) corresponding to residues in the INSERT segment in ATP_{lid} are indicated.

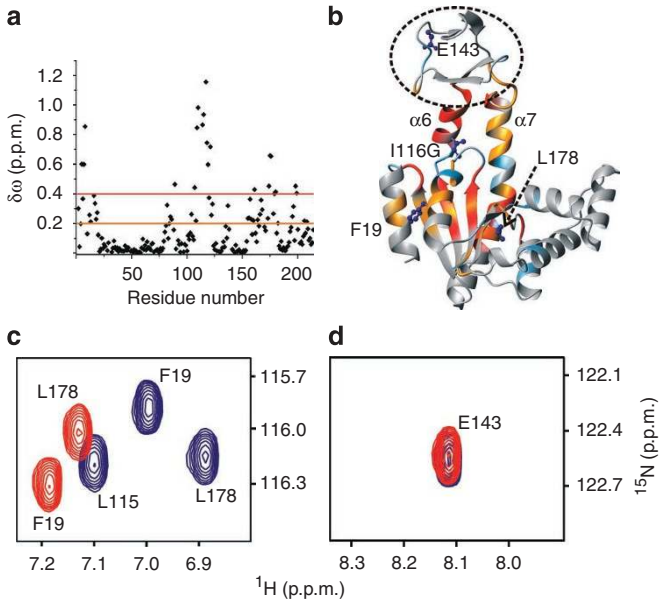

Figure 3 | Propagation of structural perturbations in the M1 mutant. Perturbations resulting from the mutation were quantified on the basis of combined absolute ^{15}N and ^{1}H chemical shift differences between WT and mutant, calculated according to $\delta\omega = 0.2 \times |\Delta^{15}N| + |\Delta^{1}H|$ (p.p.m.)[16]. As a result of the point mutation, structural rearrangements are propagated throughout the entire ATP_{lid}, with the exception of residues in the INSERT segment (indicated with a dashed oval). (**a**) Chemical shift differences for non-mutated residues plotted against the primary sequence; threshold values used in (**b**) are indicated with red and orange lines. (**b**) Chemical shift perturbations displayed on the open AK_e structure (4AKE.pdb); perturbations are colour coded as follows: red $\delta\omega > 0.4$ p.p.m., orange $0.4 > \delta\omega > 0.2$ p.p.m.; residues that are unassigned in either WT or M1 and proline residues are coloured blue. The mutation site and residues F19, E143 and L178 are shown as dark blue ball and sticks. (**c**, **d**) Expansions of ^{1}H-^{15}N HSQC spectra of WT (blue) and M1 (red) AK_e. (**c**) Chemical shift perturbations of L178 and F19 (both 0.27 p.p.m., calculated as stated above); both these residues are accordingly coloured orange in (**b**). (**d**) The chemical shift of E143 is identical in the mutant and WT spectra, consistent with identical structures in the INSERT segment.

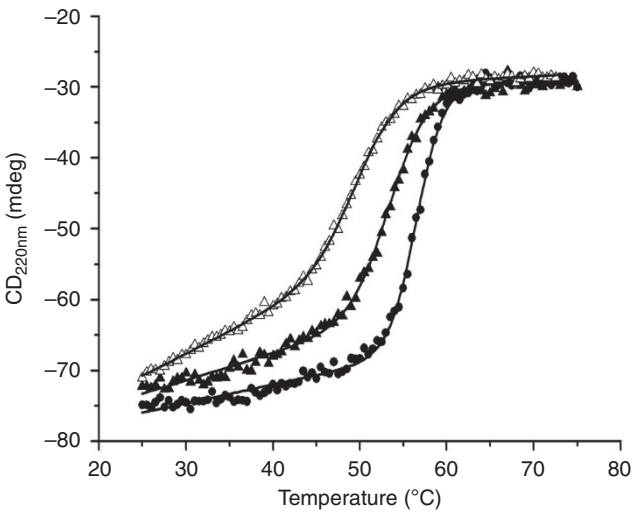

Figure 4 | Thermal denaturation of AK_e variants. Unfolding was monitored with the CD signal at 220 nm for WT (filled circles), M1 (filled triangles) and M2 (open triangles). Solid lines represent nonlinear fits to Equation (3). Fitted parameters are summarized in Supplementary Table S1.

Local unfolding promotes ATP-binding affinity. ATP-binding affinities and enthalpies between AK_e variants and ATP were determined using isothermal titration calorimetry (ITC; Fig. 5 and Table 1). All experiments were performed in duplicate and the reported parameters are average values. Surprisingly, the binding affinities of the two mutants, M1 and M2, towards ATP are increased markedly compared with WT AK_e. The observed dissociation constant (K_d^{app}) for WT is $51 \pm 13\,\mu M$ (pH 7, 25 °C), with a calorimetric enthalpy (ΔH_{ITC}) of $-2.2 \pm 0.4\,kJ\,mol^{-1}$. Binding between ATP and AK_e has previously been quantified with other biophysical techniques[16,29,30]. These independent studies provided K_d^{app} values in the range of 35–53 µM in good agreement with our ITC data. As ATP binding is associated with a low enthalpy change and baseline distortions, we performed a control experiment using Ap5A (Supplementary Fig. S2). Ap5A binds AK_e with a K_d^{app} of $0.14 \pm 0.5\,\mu M$ and a ΔH_{ITC} of $-19 \pm 5\,kJ\,mol^{-1}$, in good agreement with published results[18]. K_d^{app} values quantified for M1 and M2 are 0.78 ± 0.2 and $0.98 \pm 0.3\,\mu M$, respectively. All AK variants bind to ATP with a one-to-one stoichiometry as evident by fitted n values (Table 1), in agreement with previous NMR studies that showed one-to-one binding between WT AK_e and ATP[16]. Notably, binding of ATP to M1and M2 is associated with significantly increased ΔH_{ITC}, -51 ± 2 and $-110 \pm 10\,kJ\,mol^{-1}$, respectively. This difference is explained with a coupled folding and binding event in the case of M1 and M2, in which ΔH_{ITC} is a cumulative sum of ATP_{lid} folding (ΔH_{fol}) and ATP-binding enthalpies (ΔH_{bind}), according to Equation (1) (f_u refers to the degree of ATP_{lid} unfolding).

$$\Delta H_{ITC} = \Delta H_{bind} + f_u * \Delta H_{fol} \quad (1)$$

The structural analysis showed that helices α6 and α7 are partially unfolded in M1 and M2; thus, ΔH_{ITC} of ATP binding includes folding of these helices. The difference in calorimetric enthalpy for the two mutants scales with the degree of unfolding in ATP_{lid} observed using CD and NMR spectroscopy. The entropic term is in favour of ATP binding in the case of WT AK_e, presumably because of the release of solvent molecules hydrating both the substrate and the enzyme. In contrast, both M1 and M2 display strong enthalpy/entropy compensation for ATP binding. The large enthalpic components in M1 and M2 are paralleled with a significant entropic penalty. This may be explained by restriction of the main chain as a consequence of the coupled folding/binding event in the ATP_{lid} in these mutants.

Preservation of conformational dynamics in mutated AK_e. Chemical shifts can be used to distinguish between open and closed conformations of AK. WT AK_e in complex with Ap5A mainly populates the closed conformation[16]. The ^{1}H-^{15}N HSQC spectrum of M2, in complex with Ap5A (Supplementary Fig. S3), is of high quality and closely resembles the spectrum of Ap5A-bound WT AK_e[16]. Residues with significant chemical shift perturbations are localized to regions surrounding the sites of mutations (Supplementary Fig. S4). The similarity between WT and M2 HSQC spectra is a strong indication that M2 is adopting a structure in complex with Ap5A that closely resembles the closed AK_e conformation. Interestingly, most of the resonances that are missing (because of unfolding) in ATP_{lid} in the M2 apo state are visible and assigned in the Ap5A complex. Apparently, M2 undergoes a coupled folding and binding event on interaction with Ap5A. To directly verify that M2 is populating a closed AK_e conformation in complex with Ap5A, we made use of a chemical shift-based method previously developed in our laboratory[16]. There exists a strong linear correlation with a slope of close to unity when chemical shift perturbations between M2 and WT (both bound to Ap5A) are compared (Supplementary Fig. S5). The

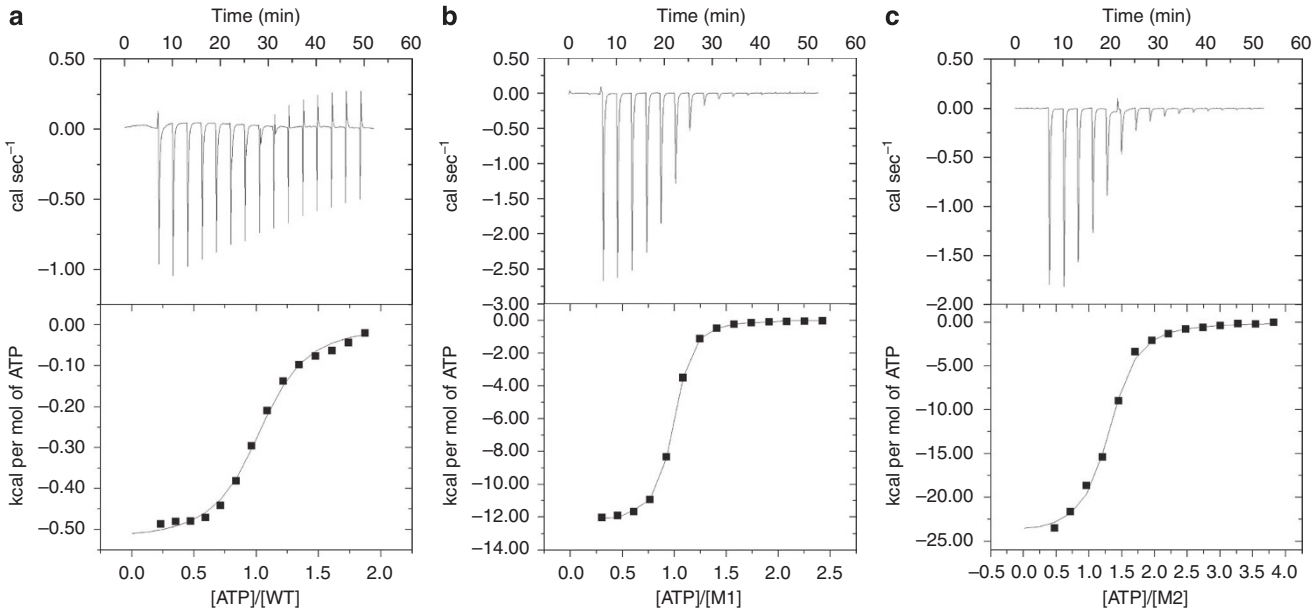

Figure 5 | Increased binding affinities towards ATP for mutated enzymes relative to WT AK_e. Apparent dissociation constants and enthalpy on binding were measured using ITC. The baseline-corrected instrumental response is shown in the upper panels, and the integrated data (squares), together with the best fits (solid lines) according to a one-site binding model, are shown in the lower panels for (**a**) WT AK_e, (**b**) M1 and (**c**) M2. Fitted parameters are summarized in Table 1.

Table 1 | ITC data for ATP binding to AK_e variants at pH 7 and 25 °C.

Protein	K_d^{app} (μM)	$\Delta H°_{ITC}$ (kJ mol^{-1})	$-T\Delta S°_{ITC}$ (kJ mol^{-1})	*n*
WT	51±13	−2.2±0.4	−22±2	1.0±0.07
M1	0.78±0.2	−51±2	16±3	0.93±0.1
M2	0.98±0.3	−110±10	75±11	1.2±0.1

linear correlation (with a slope near one) is evidence for a closed M2 conformation in complex with Ap5A, and enables the use of chemical shifts of M2 in complex with Ap5A as residue-specific markers of a fully closed enzyme. As α6 and α7 are unfolded to a degree in between M2 and WT, it is safe to assume that M1 populates a closed conformation in complex with Ap5A as well. The results show that M2 and M1 are functional enzymes that retain the ability to adopt the closed state.

Structure of AK_e:ATP complexes. The structural response to ATP binding in M1 and M2 was addressed by quantifying chemical shift perturbations in protein samples saturated with ATP. The quantitative analysis is restricted to the M1 variant as assignments of the ATP_{lid} are missing in M2. However, the ^{1}H-^{15}N HSQC spectra of ATP-saturated M1 and M2 are very similar (Supplementary Fig. S6), implying that the corresponding ATP complexes adopt similar structures. Notably, the number of observable resonances of M2 is significantly increased in the M2:ATP complex compared with the apo state (compare Fig. 2b and Supplementary Fig. S6), which is complementary evidence of a coupled folding/binding reaction, in agreement with the ITC data. In Supplementary Figures S7 and S8, the chemical shift perturbations in response to ATP binding for M1 and WT AK_e are summarized. The spatial locations of residues that are most strongly affected by ATP binding are very similar in both enzyme variants. Apparently, M1 binds to ATP with the same interaction surface as WT and as such is a functional enzyme with respect to ATP binding. This inference is valid for M2 as well, in light of the resemblance of M1 and M2 NMR spectra in ATP-saturated states.

Mutations modulate the open-to-closed equilibrium constant. We have previously shown that the ATP_{lid} in AK_e interconverts between open and closed conformations in the presence of bound ATP[16]. A detailed description of the method used to quantify populations is provided in the Supplementary Methods and in Supplementary Figures S9, S10. Equilibrium open and closed populations of both WT and the M2 variant in their ATP-bound states were determined by comparing chemical shifts in apo (open), Ap5A-bound (closed) and ATP-saturated states (Fig. 6). As assignments of ATP_{lid} in the M2 apo state was missing, the analysis was centred on the N- and C-terminal α-helices (inset Fig. 6a). Both these α-helices respond structurally to ATP binding in concert with ATP_{lid} and are valid markers of the open/closed equilibrium (Supplementary Information Fig. S2 and Table S2 in Ådén and Wolf-Watz[16]). For WT AK_e, the population of closed ATP_{lid} in the ATP complex is 0.6, in good agreement with previous analysis[16]. The fraction of closed ATP_{lid} is significantly increased in the M2:ATP complex, and, within the experimental uncertainty, the closed population is near 1. Apparently, the conformational equilibrium for the open/closed transition in the presence of ATP is strongly skewed towards the closed state as a consequence of the structural perturbation. As the NMR spectra of the ATP-saturated M1 and M2 variants are very similar, it appears likely that a similar shift in the open/closed equilibrium is valid for M1 as well.

Catalytic activities of AK_e variants. As product release is rate limiting for AK_e catalysis[10,19], the increased ATP-binding affinities of the M1 and M2 mutants are expected to hamper catalytic activities. Kinetic parameters with ATP as the variable and AMP as the constant substrate were quantified for M1, M2 and compared with that of WT AK_e (Table 2). As expected, k_{cat} values were significantly reduced (~40-fold) for the two mutants, and the reduction in k_{cat} was very close to the (50-fold) increase in

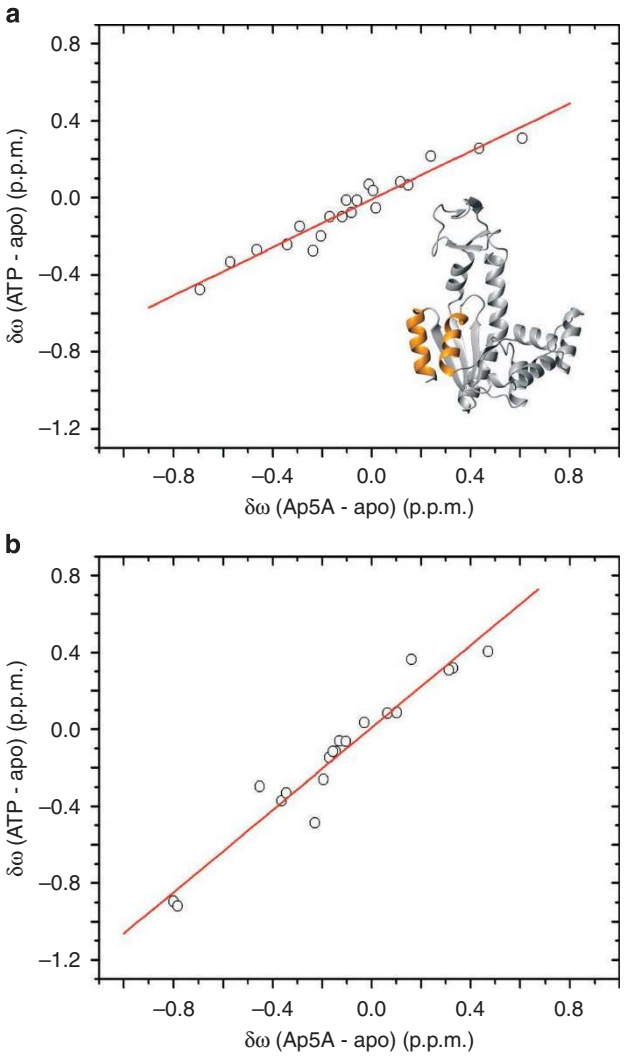

Figure 6 | Shift of open/closed equilibrium in ATP-saturated M2 versus WT AK$_e$. Normalized chemical shift perturbations in ATP- and Ap5A-bound states referenced to the apo states are calculated according to $\delta\omega = 0.2\Delta^{15}N + \Delta^{1}H$ (p.p.m.). (**a**) Correlation between ATP and Ap5A chemical shift perturbations for WT AK$_e$. The best-fitted straight line (red) has a slope of 0.62±0.07 with an *R* coefficient of 0.97. In all, 20 residues were used in the analysis. Inset: positions of the residues analysed in WT and M2 are coloured gold on the open AK$_e$ structure. (**b**) Correlation between ATP and Ap5A chemical shift perturbations for the M2 variant. The best-fitted straight line (red) has a slope of 1.07±0.1 with an *R* coefficient of 0.97; 19 residues were used in the analysis.

ATP-binding affinity. In addition, the increased ATP-binding affinities were reflected in decreased K_M^{ATP} values for the two mutants.

Discussion

The two AK$_e$ variants studied here have segmentally disordered ATP$_{lid}$ domains at 25 °C. We have previously proposed that the entire ATP$_{lid}$ functions as one cooperatively folding unit[17]. In this study, we identified additional layers in complexity in the folding behaviour of ATP$_{lid}$, namely, that α6 and α7 forms one folding unit and the INSERT segment forms a second. The mutated variants have significantly reduced vant't Hoff enthalpies of thermal unfolding but with only modest reduction in T_m. This small perturbation in T_m is a consequence of the weak thermodynamic coupling between ATP$_{lid}$ and CORE subdomains. From a functional perspective (in terms of ATP binding), the mutated variants display WT-like properties. First, the

Table 2 | Kinetic parameters for AK$_e$ catalysis with ATP as variable substrate at 25 °C.

Protein	k_{cat} (s^{-1})*	K_M^{ATP} (μM)
Wild type	390±30	50±6
M1	11±5	27±5
M2	8±4	18±6

*k_{cat} and K_M^{ATP} are determined in the direction of ADP formation.

chemical shift perturbation patterns inflicted by ATP binding are strikingly similar to the WT, showing that the same interaction surface is used for ATP interaction in mutated and WT AK$_e$. Second, both mutated variants can populate fully closed conformations in complex with the inhibitor Ap5A; thus, the enzymes retain the ability to close its substrate-binding motifs.

As a consequence of the coupled folding/binding equilibrium in the M1 and M2 variant, the enthalpic contribution for ATP binding is significantly larger compared with that of WT AKe because of the cumulative effects of folding and binding enthalpies. The decreased enthalpies of ATP binding (favouring binding) are accompanied by increased entropic components (disfavouring binding) in the mutants. Such enthalpy/entropy compensation has been observed in other proteins that mechanistically utilize coupled folding/binding reactions to interact with substrates[31].

It is remarkable that structural mutations that destabilize the ATP$_{lid}$ are paralleled with an ~50-fold increase in ATP-binding affinity. To identify the underlying molecular explanation, we analysed the formal expression for K_d^{app} following Figure 1a and obtained Equation (2) (see Supplementary Methods for derivation).

$$K_d^{app} = \frac{K_d}{1 + K_{conf}} \quad (2)$$

In Equation (2), K_d is the dissociation constant and K_{conf} is the equilibrium constant for the open-to-closed equilibrium in the presence of bound ATP (Supplementary Equation S4). An inspection of Equation (2) shows that the decreased K_d^{app} can originate from reduced K_d or increased K_{conf} values, relative to WT AK$_e$. It is unlikely that K_d is decreased in the mutants, as the structure of ATP$_{lid}$ is perturbed in both M1 and M2. On the other hand, the equilibrium constant for the open–closed transition (K_{conf}) in the presence of bound ATP is significantly skewed in the M2 variant compared with WT AK$_e$. In WT AK$_e$ and the M2 variant, the experimentally determined values of fractions closed ATP$_{lid}$ are 0.62±0.07 and 1.07±0.1, respectively. Assuming that K_d adopts equal values in WT, M1 and M2, and with a WT K_{conf} of 1.5 (0.6/0.4), Equation (2) was used to calculate a value of K_{conf} equal to 124 that accounts for the observed reduction in K_d^{app} (from ~50 μM in WT to ~1.0 μM in the mutants). This value translates to fractions of open and closed conformations of around 0 and 1, respectively, in excellent agreement with our experimental observations. Apparently, the increased affinity for ATP in the mutant AK$_e$ variants is fully explained by a large shift in the open-to-closed equilibrium constant. If, on the other hand, mutations would stabilize a 'binding incompetent state', that is, a disordered ATP$_{lid}$ on a reaction pathway towards global protein unfolding, the observed binding affinity would decrease (Supplementary Equation S6). As the ATP-binding affinity is increased as a result of the ATP$_{lid}$ destabilization, our mutations modulate the native free-energy landscape on the reaction trajectory for subdomain closure. The effect of the mutations is to redistribute states that are present in WT AK$_e$. It might seem intuitive that the chemical shifts of the mutant AK$_e$ variants should fall in between the chemical shifts of open and closed WT AK$_e$. However, a detailed consideration of chemical shifts (Supplementary Note and Supplementary Fig. S11)

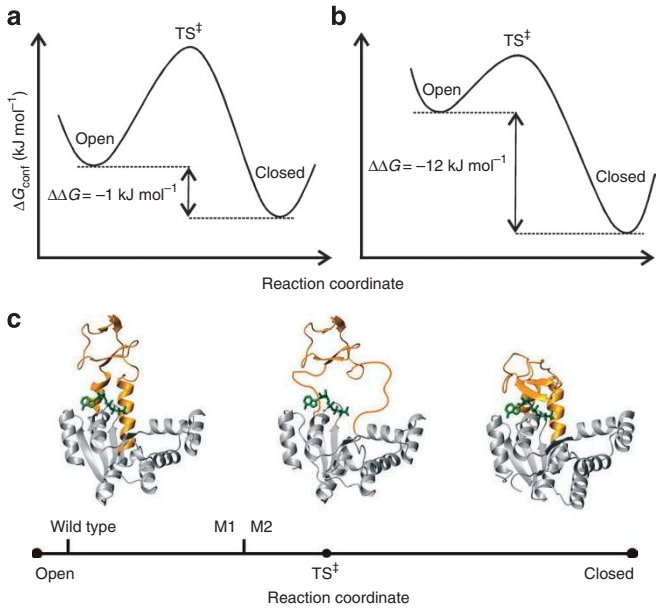

Figure 7 | Model for ATP_{lid} closure in AK_e. Relative free-energy differences between open and closed ATP_{lid} conformations in the presence of saturating ATP concentration for WT (**a**) and the M2 variant (**b**). The relative change in free energy ($\Delta\Delta G_{conf}$) is calculated from K_{conf} values of 1.5 and 124 (124 equals the minimum value that accounts for the increased ATP-binding affinity in M1 and M2 compared with WT) for WT and the M2 variant. The *y* axis in (**a**) and (**b**) is set arbitrarily such that the absolute values of the free energy for open, closed and transition state ($TS^{\ddagger}$) structures may in fact differ for the two enzymes. (**c**) Structural model of the conformational change in the ATP_{lid} in the presence of bound ATP. The ATP complex is represented with yeast AK_e in complex with the non-hydrolysable ATP analogue $AMPPCF_2P$[45]. The structures going from open to partially unfolded to closed are arranged as a function of the reaction coordinate. The relative positions of the WT and the M1, M2 variants are indicated on the reaction coordinate and should be interpreted as a qualitative measure of the distance to the transition state.

shows that this correlation is not expected. In good agreement with our model for catalysis (that is, rate-limiting dissociation of bound nucleotides), the M1 and M2 variants display ~40-fold decrease in catalytic efficiency compared with WT AK_e.

The fact that mutations redistribute already existing states is in agreement with arguments discussed previously[7]. On the basis of these arguments, we propose that local disordering of α6 and α7 is part of the reaction trajectory for closure of the ATP_{lid} (Fig. 7). As both the stable ground states (open and closed) contain well-folded α6 and α7 helices, the conformational change follows an order-disorder-order mechanism, in agreement with the cracking model[25,26]. To the best of our knowledge, this is the first experimental observation of such a mechanism. The energetic prerequisite for our mechanistic model is that the local thermodynamic stability of α6 and α7, is sufficiently low to accommodate an unfolding/folding reaction. This boundary condition has been observed for AK isolated from three different organisms[17,32]. Thus, the energetic prerequisite for our model is generally met in the AK fold. The low structural stabilities in these key regions are also reflected in high B-factors in the substrate-free AK_e structure[13,17]. Both residues mutated here (Ile 116 and Leu 168) are strongly conserved within the AK family[27]. In fact, the entire hydrophobic cluster (positions 116, 117, 164 and 168) in ATP_{lid} identified by us previously[17] is conserved with a consensus sequence equivalent to the AK_e sequence. In our proposed model, disruption of this cluster is part of the mechanism for ATP binding and, given the strong sequence conservation, the mechanism is likely to be general in the AK family. Protein folding is usually described using funnel-shaped energy landscapes[5] in which the native state exhibits minimal frustration[33]; our results with an unfolding/folding reaction during a functional transition point towards an overlap between folding and functional energy landscapes. It is possible that the novel mechanism used by AK_e during the open-to-close transition is also used by other proteins that undergo conformational changes.

A subpart of the mechanism identified for the conformational change in AK_e, that is, disorder–order transitions, has been found in interactions between proteins and a diverse set of substrates. Disorder–order mechanisms coupled to substrate binding have been observed, for instance, in protein–DNA[34], enzyme–substrate[31,35], protein–peptide[36] and protein–protein[37] interactions.

The folding of small proteins into a well-defined and compact active state is most often a highly cooperative process[38] without a significant population of non-native states. In a recent study, it was suggested that the cooperativity of the folding reaction is the result of natural selection[39]. It is intriguing that AK_e uses cooperative unfolding/refolding to accommodate a large-scale conformational change during catalysis. An appealing hypothesis is that nature has made use of cooperative unfolding/refolding to add functional properties (such as conformational plasticity) to proteins.

Methods

Protein preparation. All AK_e variants were prepared as described previously[19]. The concentrations of all proteins were determined using an extinction coefficient at 280 nm of 10.000 $M^{-1}cm^{-1}$.

Site-specific mutagenesis. Primer sequences for the M1 and M2 mutants were ordered from CyberGene. PCR-amplified DNA sequences encoding the mutant proteins were subcloned into the expression vector pET-3a (Novagen) using restriction enzymes *Nde*1 and *Bam*HI. The final constructs were verified using DNA sequencing (Eurofins MWG Operon).

Kinetic assays. Enzyme kinetic parameters for ATP turnover in the direction of ADP formation were quantified at 25 °C using a coupled spectroscopic assay[10]. The ATP concentration was varied and the AMP concentration was fixed at 0.5 mM.

NMR spectroscopy. All NMR experiments were recorded on samples containing 0.7–1.2 mM ^{15}N-labelled proteins in 50 mM NaCl and 30 mM MOPS at pH 7.0 with 10% (v/v) ^2H_2O. NMR experiments were carried out on a Bruker DRX 600 MHz spectrometer equipped with a 5-mm triple resonance *z*-gradient cryoprobe. The temperature was calibrated using an external probe inserted into the sample compartment of the NMR probe. Backbone resonance assignment of apo and substrate-saturated M1 and M2 mutants was obtained with ^{15}N nuclear overhauser effect spectroscopy-HSQC and HNHA experiments[40]. ATP and Ap5A (Sigma-Aldrich)-saturated enzymes were obtained by adding 20- and 2-mM substrate to protein samples, respectively. NMRPipe software[41] and ANSIG for Windows[42] were used for NMR data processing and visualization of spectra, respectively.

ITC. ITC experiments were carried out at 25 °C using an iTC200 Microcalorimeter (Microcal). The reference cell was filled with sample buffer, and protein-containing solutions were filled in the sample cell (200 µl volume) and titrated with ATP (40 µl). Substrate solutions were prepared in buffer (same batch) from the final step of protein purification (that is, gel filtration). Protein concentrations were 1.5 mM and 40 µM for WT titrations with ATP and Ap5A, respectively. M1 and M2 were at 20 µM for ATP titrations. The substrate concentration in the injection syringe was 10 times higher than the concentration of protein. A typical experiment consisted of an initial control injection of 1 µl, followed by 16 injections, each of 2.5 µl and 5 s duration, with a 180 s interval in between. ITC measurements were routinely taken in 50 mM NaCl and 30 mM MOPS at pH 7.0. In control experiments, the ligand (ATP) was injected into the buffer. Raw data were collected, corrected for ligand heats of dilution and integrated using the Microcal Origin software supplied with the instrument. A single-site binding model was fit to the data by a nonlinear regression analysis to yield binding constants (K_d), observed enthalpies of binding (ΔH_{ITC}) and stoichiometry of binding (n).

CD spectroscopy. Far-ultraviolet CD spectra (190–260 nm, 25 °C, 1-mm path length) and temperature scans (15–85 °C at 222 nm, 0.1-mm path length) were collected in 10 mM Na-phosphate and 50 mM NaCl (pH 7.0) on a Jasco J-810 Spectropolarimeter. Thermal denaturation curves were fitted to Equation (3) assuming a two-state reaction. The reversibility of the thermal transitions was

larger than 80%. Protein concentrations in CD experiments ranged between 5 and 10 μM.

$$S^{obs} = \frac{S_f + m_f T + (S_u + m_u T)K_u}{1 + K_u} \quad (3)$$

Where

$$K_u = \exp\left[\frac{\Delta H_{vH}(1 - \frac{T}{T_m})}{RT}\right]$$

Here, S^{obs} is the temperature-dependent spectroscopic signal, m_f, m_u and S_f, S_u are the slopes and intercepts of the folded and unfolded baselines, respectively, T is the absolute temperature, T_m is the melting point, K_u is the unfolding equilibrium constant and ΔH_{vH} is the van't Hoff enthalpy of unfolding at T_m.

References

1. Ogawa, A. *et al.* Structure of the carboxyl-terminal Src kinase, Csk. *J. Biol. Chem.* **277,** 14351–14354 (2002).
2. Debondt, H. L. *et al.* Crystal-structure of cyclin-dependent kinase-2. *Nature* **363,** 595–602 (1993).
3. Vonrhein, C., Schlauderer, G. J. & Schulz, G. E. Movie of the structural changes during a catalytic cycle of nucleoside monophosphate kinases. *Structure* **3,** 483–490 (1995).
4. Ikura, M. *et al.* Solution structure of a calmodulin-target peptide complex by multidimensional NMR. *Science* **256,** 632–638 (1992).
5. Leopold, P. E., Montal, M. & Onuchic, J. N. Protein folding funnels: a kinetic approach to the sequence-structure relationship. *Proc. Natl Acad. Sci. USA* **89,** 8721–8725 (1992).
6. Frauenfelder, H., Sligar, S. G. & Wolynes, P. G. The energy landscapes and motions of proteins. *Science* **254,** 1598–1603 (1991).
7. del Sol, A., Tsai, C. J., Ma, B. Y. & Nussinov, R. The origin of allosteric functional modulation: multiple pre-existing pathways. *Structure* **17,** 1042–1050 (2009).
8. Gerstein, M., Lesk, A. M. & Chothia, C. Structural mechanisms for domain movements in proteins. *Biochemistry* **33,** 6739–6749 (1994).
9. Noda, L. Adenylate kinase. in *The Enzymes* (ed. Boyer, P. D.) 279–305 (VIII, Academic Press, 1973).
10. Rhoads, D. G. & Lowenstein, J. M. Initial velocity and equilibrium kinetics of myokinase. *J. Biol. Chem.* **243,** 3963–3972 (1968).
11. Sheng, X. R., Li, X. & Pan, X. M. An iso-random Bi Bi mechanism for adenylate kinase. *J. Biol. Chem.* **274,** 22238–22242 (1999).
12. Abele, U. & Schulz, G. E. High-resolution structures of adenylate kinase from yeast ligated with inhibitor Ap5A, showing the pathway of phosphoryl transfer. *Protein Sci.* **4,** 1262–1271 (1995).
13. Müller, C. W., Schlauderer, G. J., Reinstein, J. & Schulz, G. E. Adenylate kinase motions during catalysis: an energetic counterweight balancing substrate binding. *Structure* **4,** 147–156 (1996).
14. Lienhard, G. E. & Secemski, I. I. P 1,P 5-Di(adenosine-5′)pentaphosphate, a potent multisubstrate inhibitor of adenylate kinase. *J. Biol. Chem.* **248,** 1121–1123 (1973).
15. Müller, C. W. & Schulz, G. E. Structure of the complex between adenylate kinase from *Escherichia coli* and the inhibitor Ap5A refined at 1.9 Å resolution. A model for a catalytic transition state. *J. Mol. Biol.* **224,** 159–177 (1992).
16. Ådén, J. & Wolf-Watz, M. NMR identification of transient complexes critical to adenylate kinase catalysis. *J. Am. Chem. Soc.* **129,** 14003–14012 (2007).
17. Rundqvist, L. *et al.* Noncooperative folding of subdomains in adenylate kinase. *Biochemistry* **48,** 1911–1927 (2009).
18. Schrank, T. P., Bolen, D. W. & Hilser, V. J. Rational modulation of conformational fluctuations in adenylate kinase reveals a local unfolding mechanism for allostery and functional adaptation in proteins. *Proc. Natl Acad. Sci. USA* **106,** 16984–16989 (2009).
19. Wolf-Watz, M. *et al.* Linkage between dynamics and catalysis in a thermophilic-mesophilic enzyme pair. *Nat. Struct. Mol. Biol.* **11,** 945–949 (2004).
20. Henzler-Wildman, K. A. *et al.* Intrinsic motions along an enzymatic reaction trajectory. *Nature* **450,** 838–844 (2007).
21. Boehr, D. D., McElheny, D., Dyson, H. J. & Wright, P. E. The dynamic energy landscape of dihydrofolate reductase catalysis. *Science* **313,** 1638–1642 (2006).
22. Eisenmesser, E. Z. *et al.* Intrinsic dynamics of an enzyme underlies catalysis. *Nature* **438,** 117–121 (2005).
23. Beach, H., Cole, R., Gill, M. L. & Loria, J. P. Conservation of mus-ms enzyme motions in the apo- and substrate-mimicked state. *J. Am. Chem. Soc.* **127,** 9167–9176 (2005).
24. Gerstein, M., Schulz, G. & Chothia, C. Domain closure in adenylate kinase. Joints on either side of two helices close like neighboring fingers. *J. Mol. Biol.* **229,** 494–501 (1993).
25. Miyashita, O., Onuchic, J. N. & Wolynes, P. G. Nonlinear elasticity, proteinquakes, and the energy landscapes of functional transitions in proteins. *Proc. Natl Acad. Sci. USA* **100,** 12570–12575 (2003).
26. Whitford, P. C., Miyashita, O., Levy, Y. & Onuchic, J. N. Conformational transitions of adenylate kinase: switching by cracking. *J. Mol. Biol.* **366,** 1661–1671 (2007).
27. Henzler-Wildman, K. A. *et al.* A hierarchy of timescales in protein dynamics is linked to enzyme catalysis. *Nature* **450,** 913–916 (2007).
28. Monnot, M. *et al.* Circular dichroism investigation of *Escherichia coli* adenylate kinase. *J. Biol. Chem.* **262,** 2502–2506 (1987).
29. Sanders, C. R. II, Tian, G. C. & Tsai, M. D. Mechanism of adenylate kinase. Is there a relationship between local substrate dynamics, local binding energy, and the catalytic mechanism? *Biochemistry* **28,** 9028–9043 (1989).
30. Reinstein, J. *et al.* Fluorescence and NMR investigations on the ligand binding properties of adenylate kinases. *Biochemistry* **29,** 7440–7450 (1990).
31. McElroy, C. A., Manfredo, A., Gollnick, P. & Foster, M. P. Thermodynamics of tryptophan-mediated activation of the trp RNA-binding attenuation protein. *Biochemistry* **45,** 7844–7853 (2006).
32. Krishnamurthy, H., Munro, K., Yan, H. & Vieille, C. Dynamics in Thermotoga neapolitana adenylate kinase: 15N relaxation and hydrogen-deuterium exchange studies of a hyperthermophilic enzyme highly active at 30 degrees C. *Biochemistry* **48,** 2723–2739 (2009).
33. Bryngelson, J. D. & Wolynes, P. G. Spin glasses and the statistical mechanics of protein folding. *Proc. Natl Acad. Sci. USA* **84,** 7524–7528 (1987).
34. Berger, C., Jelesarov, I. & Bosshard, H. R. Coupled folding and site-specific binding of the GCN4-bZIP transcription factor to the AP-1 and ATF/CREB DNA sites studied by microcalorimetry. *Biochemistry* **35,** 14984–14991 (1996).
35. Keramisanou, D. *et al.* Disorder-order folding transitions underlie catalysis in the helicase motor of SecA. *Nat. Struct. Mol. Biol.* **13,** 594–602 (2006).
36. Cliff, M. J., Williams, M. A., Brooke-Smith, J., Barford, D. & Ladbury, J. E. Molecular recognition via coupled folding and binding in a TPR domain. *J. Mol. Biol.* **346,** 717–732 (2005).
37. Radhakrishnan, I. *et al.* Solution structure of the KIX domain of CBP bound to the transactivation domain of CREB: a model for activator:coactivator interactions. *Cell* **91,** 741–752 (1997).
38. Jackson, S. E. & Fersht, A. R. Folding of chymotrypsin inhibitor 2. 1. Evidence for a two-state transition. *Biochemistry* **30,** 10428–10435 (1991).
39. Watters, A. L. *et al.* The highly cooperative folding of small naturally occurring proteins is likely the result of natural selection. *Cell* **128,** 613–624 (2007).
40. Vuister, G. W. & Bax, A. Quantitative J correlation: a new approach for measuring homonuclear 3-bond J(H(N)H(alpha) coupling-constants in N-15-enriched proteins. *J. Am. Chem. Soc.* **115,** 7772–7777 (1993).
41. Delaglio, F. *et al.* NMRPipe: a multidimensional spectral processing system based on UNIX pipes. *J. Biomol. NMR* **6,** 277–293 (1995).
42. Helgstrand, M., Kraulis, P., Allard, P. & Härd, T. Ansig for Windows: an interactive computer program for semiautomatic assignment of protein NMR spectra. *J. Biomol. NMR* **18,** 329–336 (2000).
43. Shapiro, Y. E., Sinev, M. A., Sineva, E. V., Tugarinov, V. & Meirovitch, E. Backbone dynamics of *Escherichia coli* adenylate kinase at the extreme stages of the catalytic cycle studied by (15)N NMR relaxation. *Biochemistry* **39,** 6634–6644 (2000).
44. Koradi, R., Billeter, M. & Wüthrich, K. MOLMOL: a program for display and analysis of macromolecular structures. *J. Mol. Graph.* **14,** 51–55, 29–32 (1996).
45. Schlauderer, G. J., Proba, K. & Schulz, G. E. Structure of a mutant adenylate kinase ligated with an ATP-analogue showing domain closure over ATP. *J. Mol. Biol.* **256,** 223–227 (1996).

Acknowledgments

This research was financially supported by an Umeå University 'Young researcher award' (M.W.-W.) and by the Kempe foundation (U.O. and M.W-W.). We thank Pernilla Wittung-Stafshede for fruitful discussions during the project and for critically reviewing the manuscript.

Author contributions

U.O. designed and conducted the experiments and analysed the data, M.W.-W. designed the experiments, analysed the data and wrote the manuscript.

Additional information

Supplementary Information accompanies this paper on http://www.nature.com/naturecommunications

Competing financial interests: The authors declare no competing financial interests.

Reprints and permission information is available online at http://npg.nature.com/reprintsandpermissions/

How to cite this article: Olsson, U. & Wolf-Watz, M. Overlap between folding and functional energy landscapes for adenylate kinase conformational change. *Nat. Commun.* 1:111 doi: 10.1038/ncomms1106 (2010).